



Open Archive TOULOUSE Archive Ouverte (OATAO)

OATAO is an open access repository that collects the work of Toulouse researchers and makes it freely available over the web where possible.

This is an author-deposited version published in : <http://oatao.univ-toulouse.fr/>
Eprints ID : 10220

To cite this version : Bonometti, Thomas and Izard, Edouard and Lacaze, Laurent *Resolved simulations of submarine avalanches with a simple soft-sphere / immersed boundary method.* (2013) In: 8th International Conference on Multiphase Flow - ICMF 2013, 26 May 2013 - 31 May 2013 (Jeju, Korea, Republic Of).

Any correspondence concerning this service should be sent to the repository administrator: staff-oatao@listes-diff.inp-toulouse.fr

Resolved simulations of submarine avalanches with a simple soft-sphere / immersed boundary method

Thomas Bonometti, Edouard Izard, Laurent Lacaze

*IMFT, Université de Toulouse, INPT, UPS, CNRS, Institut de Mécanique des Fluides de Toulouse,
Allée Camille Soula, F-31400 Toulouse, France*

Keywords: immersed boundary, discrete element method, submarine avalanches, resolved simulations

Abstract

Physical mechanisms at the origin of the transport of solid particles in a fluid are still a matter of debate in the physics community. Yet, it is well known that these processes play a fundamental role in many natural configurations, such as submarine landslides and avalanches, which may have a significant environmental and economic impact. The goal here is to reproduce the local dynamics of such systems from the grain scale to that of thousands of grains approximately. To this end a simple soft-sphere collision / immersed-boundary method has been developed in order to accurately reproduce the dynamics of a dense granular media collapsing in a viscous fluid. The fluid solver is a finite-volume method solving the three-dimensional, time-dependent Navier-Stokes equations for an incompressible flow on a staggered grid. Here we use a simple immersed-boundary method consisting of a direct forcing without using any Lagrangian marking of the boundary, the immersed boundary being defined by the variation of a solid volume fraction from zero to one. The granular media is modeled with a discrete element method (DEM) based on a multi-contact soft-sphere approach. In this method, an overlap is allowed between spheres which mimics the elasto-plastic deformation of real grain, and is used to calculate the contact forces based on a linear spring model and a Coulomb criterion. Binary wall-particle collisions in a fluid are simulated for a wide range of Stokes number ranging from 10^{-1} to 10^4 . It is shown that good agreement is observed with available experimental results for the whole range of investigated parameters, provided that a local lubrication model is used when the distance of the gap between the particles is below a fraction of the particle radius. A new model predicting the coefficient of restitution as a function of the Stokes number and the relative surface roughness of the particles is proposed. This model, which makes use of no adjustable constant, is shown to be in good agreement with available experimental data. Finally, simulations of dense granular flows in a viscous fluid are performed. The present results are encouraging and open the way for a parametric study in the parameter space initial aspect ratio - initial packing.

Introduction

Particle-laden flows are encountered in a large number of industrial and natural applications, including chemical engineering, aeronautics, transportations, biomechanics, geophysics and oceanography. Modeling solid-fluid interaction is often difficult because of the complexity of the solid shape and motion in the fluid flow.

Methods for modeling solid-fluid interaction may be divided within two main groups, depending on the way the solid-fluid interfaces are described. One group, usually referred to as "body-fitted grid methods" makes use of a structured curvilinear or unstructured grid to conform the grid to the boundary of the fluid domain (Moin and Mahesh 1998; Hu et al. 2001). In situations involving complex moving boundaries, one needs to establish a new body-conformal grid at each time-step which leads to a substantial computational cost and subsequent slowdown of the solution procedure. In addition, issues associated with regridding arise such as grid-quality and grid-interpolation errors.

The second group of methods is referred to as "fixed-grid methods". These techniques make use of a fixed grid, which eliminates the need of regridding, while the presence of the

solid objects is taken into account via adequately formulated source terms added to fluid flow equations. Fixed-grid methods have emerged in recent years as a viable alternative to body-conformal grid methods. In this group, one can mention immersed-boundary method (IBM) (Peskin 2000; Fadlun et al. 2000; Kim et al. 2001; Uhlmann 2005), among others.

In the present work, we attempt to simulate the local dynamics of such systems from the grain scale to that of thousands of grains approximately. To this end a simple soft-sphere collision / immersed-boundary method is presented. The immersed-boundary method consists in a direct forcing method, using a continuous solid volume fraction to define the boundary. The granular media is modeled with a discrete element method (DEM) based on a multi-contact soft-sphere approach.

The paper is structured as follows. First we describe the numerical techniques used here, then preliminary test cases are presented to show the ability of both methods independently. In a third part, binary wall-particle collisions in a fluid are simulated for a wide range of Stokes number ranging from 10^{-1} to 10^4 , and a discussion about the use of a local lubrication model is done. In addition, a new model predicting the coefficient of restitution as a function of the

Stokes number and the relative surface roughness of the particles is proposed. Finally, simulations of dense granular flows in a viscous fluid are presented.

Nomenclature

g	gravitational constant (ms ⁻²)
p	pressure (Nm ⁻²)
R	mean particle radius (m)
D	mean particle diameter (m)
V	local velocity in the fluid (ms ⁻¹)
u_p	particle velocity (ms ⁻¹)
U	local velocity in the particle (ms ⁻¹)
F	IBM volume force (ms ⁻²)
v_p^3	particle volume (m ³)
m_p	particle mass (kg)
e_n	coefficient of normal restitution
t_c	contact time (s)

Greek letters

α	solid volume fraction
μ	dynamic viscosity (Pa s)
ν	kinematic viscosity (m ² s ⁻¹)
ρ	density (kg m ⁻³)

Subscripts

p	particle
f	fluid

Numerical Approaches

Immersed-boundary method (IBM)

Assuming a Newtonian fluid, the evolution of the flow is described using the Navier-Stokes equations, namely

$$\nabla \cdot \mathbf{V} = 0 \quad (1)$$

$$\rho \frac{\partial \mathbf{V}}{\partial t} + \rho \mathbf{V} \cdot \nabla \mathbf{V} = -\nabla p + \rho \mathbf{g} + \nabla \cdot [\mu(\nabla \mathbf{V} + {}^t \nabla \mathbf{V})] + \rho \mathbf{f} \quad (2)$$

where \mathbf{V} , p , ρ and μ are the local velocity, pressure, density and dynamic viscosity in the flow, respectively, \mathbf{g} denotes gravity and \mathbf{f} is a volume force term used to take into account solid-fluid interaction. (1)-(2) are written in a Cartesian or polar system of coordinates. These equations are enforced throughout the entire domain, comprising the actual fluid domain and the space occupied by the particles. In the following, the term \mathbf{f} will be formulated in such way as to represent the action of the immersed solid boundaries upon the fluid.

Let us consider a non-deformable solid particle of density ρ_p , volume v_p^3 and mass m_p , the centroid of which being located at \mathbf{x}_p , moving at linear and angular velocity \mathbf{u}_p and $\boldsymbol{\omega}_p$, respectively. The local velocity \mathbf{U} in the object is then defined by $\mathbf{U} = \mathbf{u}_p + \mathbf{r} \times \boldsymbol{\omega}_p$, \mathbf{r} being the local position relative the solid centroid. The motion of the particle is described by Newton's equations for linear and angular momentum of a rigid body, *viz* (Uhlmann 2005),

$$m_p \frac{d\mathbf{u}_p}{dt} = m_p \mathbf{g} + \mathbf{F}_h \quad \mathbf{I}_p \frac{d\boldsymbol{\omega}_p}{dt} = \boldsymbol{\Gamma}_h \quad (3)$$

with

$$\mathbf{F}_h = - \frac{\rho \rho_p}{(\rho_p - \rho)} \int_{\vartheta_p} \mathbf{f} d\vartheta \quad (4)$$

$$\boldsymbol{\Gamma}_h = - \frac{\rho \rho_p}{(\rho_p - \rho)} \int_{\vartheta_p} \mathbf{r} \times \mathbf{f} d\vartheta \quad (5)$$

where \mathbf{F}_h (resp. $\boldsymbol{\Gamma}_h$) is the acceleration (resp. torque) due to hydrodynamic forces.

The time integration of the momentum equations for the fluid (2) and the solid (3) is performed via a third-order Runge-Kutta method for all terms except the viscous term for which a second-order semi-implicit Crank-Nicolson scheme is used. The incompressibility condition (1) is satisfied at the end of each time step through a projection method. Domain decomposition and Message Passing Interface (MPI) parallelization is performed to facilitate simulation of large number of computational cells.

In general, the location of the particle surface is unlikely to coincide with the grid nodes, so that interpolation techniques are usually employed to enforce the boundary condition by imposing constraints on the neighboring grid nodes. Here we adopt another strategy, by introducing a function α denoted as "solid volume fraction", which is equal to one in cells filled with the solid phase, zero in cells filled with the fluid phase, and $0 < \alpha < 1$ in the region of the boundary. In practice, the transition region is set-up to be of one-to-three grid cells approximately (Yuki et al. 2007). The forcing term reads

$$\mathbf{f} = \alpha \frac{\mathbf{U} - \mathbf{V}}{\Delta t} \quad (6)$$

Recall that \mathbf{U} is the local velocity imposed to the immersed solid object while \mathbf{V} is the local velocity in the fluid; Δt is the time step used for the time-advancement. The present choice, which may be viewed as a smoothing of the immersed boundary, is an alternative way to using a regularized delta function in conjunction with a Lagrangian marking of the boundary. The latter technique is largely used in immersed-boundary methods in order to allow for a smooth transfer of momentum from the boundary to the fluid (see e.g. Fadlun et al. 2000; Uhlmann 2005). The advantage of the present choice is that (1) it is simple to implement, (2) there is no need to introduce any Lagrangian mesh for tracking the immersed boundary, (3) no interpolation is performed so that the computational cost is reduced.

In the following, spherical particles will be considered. The corresponding solid volume fraction α is defined by (Yuki et al. 2007),

$$\alpha(\mathbf{x}) = \frac{1}{2} - \frac{1}{2} \tanh \left(\frac{|\mathbf{x} - \mathbf{x}_p| - R}{\lambda \sigma \Delta} \right) \quad (7)$$

$$\lambda = |n_x| + |n_y| + |n_z| \quad (8)$$

$$\sigma = 0.065 (1 - \lambda^2) + 0.39 \quad (9)$$

where $\mathbf{n} = (n_x, n_y, n_z)$ is a normal outward unit vector at a surface element, σ is a parameter controlling the thickness of the transition region and Δ is a characteristic grid size ($\Delta = 2^{1/2} \Delta x$ when the grid is uniform). Iso-contours of α as defined in (7) are shown in figure 2. With the present choices, the transition region is of three grid cells approximately.

Soft-sphere approach (DEM)

In this section, we describe the method used for dealing with solid contacts in a system of n_p particles. Here, the modeling of the solid-solid interaction is done via a soft-sphere approach. Briefly, we assume the particles to be non-deformable but being able to overlap each other. This overlap is then used to compute the normal and tangential contact forces, using a local linear mass-spring system and a Coulomb type model, respectively. When coupling is performed, an extra force \mathbf{F}_c and torque $\mathbf{\Gamma}_c$ is added in (3), namely

$$\mathbf{F}_c = \sum_{j \neq i} \mathbf{F}_{i-j} + \mathbf{F}_{wall} \quad (10)$$

$$\mathbf{\Gamma}_c = \sum_{j \neq i} \mathbf{\Gamma}_{i-j} + \mathbf{\Gamma}_{wall} \quad (11)$$

where \mathbf{F}_{i-j} is the contact force between particles i and j , \mathbf{F}_{wall} the wall-particle interaction force, $\mathbf{\Gamma}_{i-j}$ and $\mathbf{\Gamma}_{wall}$ are the corresponding torques. \mathbf{F}_{i-j} and $\mathbf{\Gamma}_{i-j}$ are computed using a local system of coordinates (\mathbf{n}, \mathbf{t}) depicted in figure 1 as follows

$$\mathbf{F}_{i-j} = F_n \mathbf{n} + F_t \mathbf{t} \quad (12)$$

$$\mathbf{\Gamma}_{i-j} = R_i \mathbf{n} \times F_t \mathbf{t} \quad (13)$$

$$F_n = \begin{cases} 0 & \text{if } \delta_n > 0 \\ \max\left(0, -k_n \delta_n - \gamma_n \frac{d\delta_n}{dt}\right) & \text{otherwise} \end{cases} \quad (14)$$

$$F_t = -\min(|k_t \delta_t|, \mu_c F_n) \text{sign}(\delta_t) \quad (15)$$

where R_i is the i -th particle radius, δ_n (δ_t) is the normal (tangential) distance of overlap, μ_c is the friction coefficient, k_n (k_t) is the normal (tangential) stiffness and γ_n is the damping coefficient of the mass-spring model, respectively. Note that \mathbf{F}_{wall} and $\mathbf{\Gamma}_{wall}$ are treated in a similar manner by taking an infinite radius and mass for the wall. The constants of the mass-spring model γ_n , k_n and k_t are calculated thanks to two additional parameters, namely the coefficient of normal restitution e_n and the contact time t_c . These quantities are characteristic of the elastic properties of the particles.

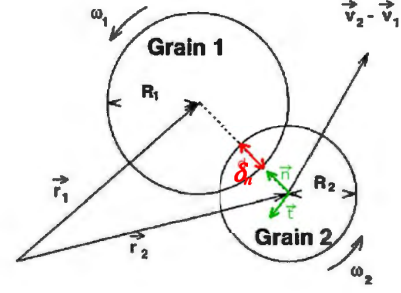


Figure 1: Notations used in the soft-sphere approach.

$$\gamma_n = -\frac{2m_*}{t_c} \ln(e_n) \quad (16)$$

$$k_n = \frac{m_* \pi^2}{t_c^2} + \frac{\gamma_n^2}{4m_*} \quad (17)$$

where $m_* = m_i m_j / (m_i + m_j)$ is the effective mass involved in the contact. Finally, the tangential stiffness coefficient k_t is assumed to be proportional to the normal stiffness coefficient k_n (Foerster et al. 1994). In the present work, we set $k_t = 0.2 k_n$. To summarize, in the present soft-sphere approach, one needs to specify e_n , t_c and μ_c in addition to the size and density of the particles for the model to be closed.

Lubrication force

As shown later, the coupled IBM-DEM method may not be accurate in capturing the detailed flow structure in the liquid film which is drained when the particles approach each other because of the somewhat limited spatial resolution of the flow in the narrow gap. An extra lubrication force may thus be used in (3) to compensate for this (Kempe et al. 2012). Here we use the following model of lubrication force between two approaching particles i and j of velocity \mathbf{u}_{pi} and \mathbf{u}_{pj} and radius R_i and R_j (Brenner 1961),

$$\mathbf{F}_{lub} = -\frac{6\pi\mu (\mathbf{u}_{pi} \cdot \mathbf{n} - \mathbf{u}_{pj} \cdot \mathbf{n})}{\delta_n + \eta} \left(\frac{R_i R_j}{R_i + R_j} \right)^2 \mathbf{n} \quad (18)$$

where η is an effective roughness length accounting for the surface roughness of real grains. This parameter was added in the model in order to mimic real particles and avoid the divergence of the force when contact occurs ($\delta_n = 0$). Depending on the type of material used for the particles, the relative surface roughness η/R is roughly in the range $[10^{-6}; 10^{-3}]$ (Joseph et al. 2001). The present lubrication force is used when the distance between particles is in the range $0 \leq \delta_n \leq R/2$. We checked that the specific value of the upper bound of the force application (within the range $[\Delta x; R]$) did not affect the results significantly. Results with the lubrication force (18) are presented in figures 4-5 and 7-8.

Preliminary tests without coupling

Falling sphere in a viscous liquid initially at rest

We set the physical properties of the particle and the fluid so the density ratio is $\rho_p/\rho = 4$ and the Archimedes number $Ar = \rho(\rho_p - \rho)gD^3/\mu^2 = 800$. As shown later, this corresponds to a Reynolds number, based on the terminal velocity of the sphere, of $Re = \rho u_p D/\mu = 20$ approximately. Here, we compare our results with those of a boundary-fitted approach which has been validated in previous papers (Mougin & Magnaudet 2001). This method fully resolves the flow around the falling sphere in the reference frame of the moving object, thanks to a spherical curvilinear grid which is refined in the vicinity of the rigid boundary. The particle motion is solved via the Kirchhoff equations of motion. In this method a $88 \times 34 \times 66$ spherical grid is used and the outer boundary are located at a distance of $20D$ from the sphere center.

As for the present method, the simulation is performed in a cylindrical computational (r, z) -domain of $20D \times 40D$ size with a 128×800 grid points. The spatial resolution is constant along the z -direction parallel to gravity as well as in the region $0 \leq r/D \leq 1.5$ ($D/\Delta x = 20$). For $1.5 \leq r/D \leq 20$, the grid size is varied following an arithmetic progression up to the outer wall. Free-slip boundary conditions are imposed at all boundaries. The time-step used for the simulation is $\Delta t(g/D)^{1/2} = 0.04$. Figure 2 shows the grid used and iso-contours of the solid volume fraction α defined in (7). The sphere is initially located at a distance $5R$ from the upper wall and the fluid is initially at rest.

One can estimate the initial acceleration of the sphere at early times, assuming that only the buoyancy force and the added-mass force are at play. The initial vertical acceleration reads

$$\frac{du_p}{dt} = \frac{(\rho_p - \rho)g}{\rho_p + C_M \rho} \quad (19)$$

where C_M is the added-mass coefficient equal to $1/2$ for a sphere. When the sphere has reached a terminal velocity, the drag force is balanced by the buoyancy force so the terminal velocity can be computed as follows

$$u_p = \sqrt{\frac{|m_p - m|g}{C_D \frac{1}{2} \rho \pi R^2}} \quad (20)$$

where m_p and m are the mass of the spherical particle and that of the fluid contained in an equivalent volume, respectively. C_D is the drag coefficient which can be classically estimated using Schiller and Naumann's correlation (Clift et al. 1978). Using this correlation together with the definition of the Reynolds number $Re = \rho u_p D/\mu$ and (20), one can compute the terminal velocity of the sphere. Figure 2 shows the temporal evolution of the sphere velocity with the boundary-fitted approach and the present immersed boundary method. For comparison, analytical solutions (19) and (20) are also plotted. Excellent agreement is observed with respect to both the numerical and analytical solutions. The present method is shown to satisfactorily reproduce the dynamics of a free-moving object in a viscous fluid, from

the acceleration phase up to the steady-state regime.

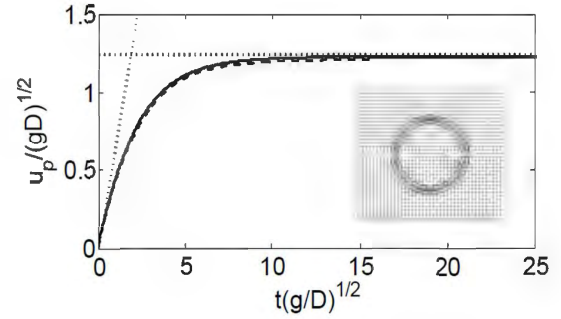


Figure 2: Time evolution of the particle velocity: —, present IBM method, - - -, boundary-fitted approach, ·····, analytical solutions (19)-(20). Inset: close-up view of the grid used for the IBM simulation, with iso-contours of $\alpha = 0.01, 0.25, 0.5, 0.75$ and 0.99 .

Granular pressure in silo

In this section, only the soft-sphere approach is used, that is we solve (3) after having replaced F_h and Γ_h by F_c and Γ_c , respectively. This test case correspond to the filling of a silo of dimension $0.1 \times 0.1 \times 5$ m (figure 3) by 56000 particles of density $\rho_p = 1317 \text{ kg.m}^{-3}$ and mean radius $R = 5 \times 10^{-3}$ m under gravity $g = 9.81 \text{ m/s}^2$. The radius is varied from one particle to another in a range of $\pm 10\%$ to avoid crystallization phenomena. Here we set the collision parameters to $\mu_c = 0.25$, $e_n = 0.3$ and $t_c = 10^{-4}$ s. The walls of the silo were covered by fixed particles of equivalent size as those injected in the silo.

When the granular column is at rest, a coarse-graining technique is applied (see e.g. Goldhirsch & Goldenberg 2002) to measure the local granular stress tensor and the subsequent granular pressure (spherical part of the tensor). We plot on figure 3 the horizontally-averaged granular pressure in the silo. Going from the top of the column ($z \approx 5$ m) down to the bottom ($z = 0$ m), the granular pressure first follows a “hydrostatic” linear distribution on a depth corresponding to one silo diameter ($4.9\text{m} \leq z \leq 5$ m), then the pressure quickly reaches a plateau and remains roughly constant on a distance of 4m down to $z \approx 0.7$ m. Below this height, the pressure monotonously increases as one gets to the bottom boundary. This behavior is attributed to the fact that in this region, particles have interacted with the bottom wall so the friction with the vertical wall was reduced and the pressure increased accordingly.

The prediction of the granular pressure in the silo has been the subject of considerable work because of its obvious practical interest. One conventional model, namely the Janssen model, has proved to reproduce reasonably well the pressure distribution in a silo. In this model one assumes that (i) the grain assembly is a continuous medium of equivalent density $\rho_{gm} = C\rho_p$, C being the global compactness in the granular column, (ii) the vertical stresses are redistributed toward the horizontal directions by a factor K and (iii) the wall friction is at the threshold of motion. Under these assumption, the vertical distribution of the granular pressure reads,

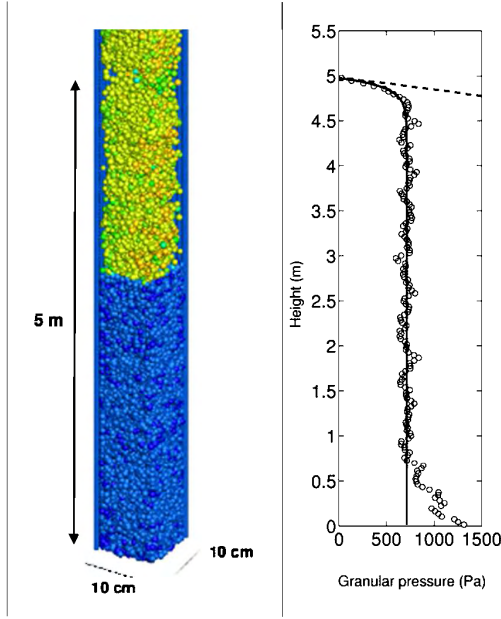


Figure 3: Soft-sphere simulation. (Left) Silo filling with 56000 particles colorized by their velocity (blue: low velocity, red: high velocity). (Right) Horizontally-averaged granular pressure distribution in the silo (when the granular medium is at rest): \circ , present DEM method, —, analytical solution (21), - - -, equivalent hydrostatic distribution.

$$p(z) = \frac{\rho_{gm} g S}{f_w K P} \left(1 - e^{-\frac{f_w K P}{S}(h-z)} \right) \quad (21)$$

where $S(P)$ is the horizontal section (perimeter) of the silo, f_w is the wall friction coefficient, K is the coefficient of stress redirection and h is the height of the granular column. Note that the coarse-graining technique allows us to directly measure f_w and K while these quantities are difficult to determine a priori or in a real experiment. Therefore, we plotted in figure 3 the analytical solution (21) by estimating the parameter $f_w K$ using a best fit of the numerical results. This gives a value of $f_w K \approx 0.30 \pm 0.06$. The direct calculation of $f_w K$ from the numerical data gives, including the dispersion error, $f_w K \approx 0.38 \pm 0.11$, a value which is in reasonable agreement with the best-fit estimate. This shows the capability of the present soft-sphere method to accurately reproduce the behavior of a dense granular media in motion and at rest.

Results and Discussion

Bouncing of a solid sphere on a wall in a viscous fluid

In this section, we present results of the simulation of one spherical particle bouncing on a wall in a viscous liquid initially at rest. To this end, the immersed boundary method (IBM) is coupled with the soft-sphere approach (DEM). The simulation is performed with the same grid as that used in figure 2. Here the resolution is $D/\Delta x = 20$. Note that tests with $D/\Delta x = 10$ and 40 have been done and showed that the

results were not affected by spatial resolution. Free-slip boundary conditions are imposed at all boundaries except at the bottom wall where bouncing occurs. We set the physical properties of the particle and the fluid so that we cover a large range of density ratios $2 \leq \rho_p/\rho_f \leq 10^2$, Reynolds numbers $0.1 \leq Re = \rho_f u_p D/\mu \leq O(10^3)$ and Stokes numbers $1 \leq St \leq 10^4$. Here Stokes number is defined as,

$$St = \frac{(\rho_p + C_M \rho) V_T D}{9\mu} \quad (22)$$

where $C_M = 1/2$ is the added-mass coefficient of the spherical particle.

The evolution of the vorticity field around the particle during impact is presented in figure 4, for the case $\rho_p/\rho_f = 8$, $St = 53$ and $Re = 60$. Here the collision parameters were set to $e_n = 0.97$, $t_c = 10^{-4}$ s, $\mu_c = 0.25$, and the relative surface roughness used in the lubrication model (18) was set to $\eta/R = 4 \times 10^{-4}$. At $t = 19.74$, the flow field around the particle is not influenced by the wall and vice versa. However, when the sphere gets closer to the wall, the fluid is pushed away from the centerline and vorticity is created at the wall. This is visible in figure 4 at time $t = 19.89$ as the particle is at a distance from the wall of R approximately. Note that at this time instance, the grid resolution is of 4-5 grid cells in the liquid film. When collision occurs at $t = 20.02$ ($\delta_n \leq 0$), vorticity is maximum in the region close to the impact zone, indicating strong shear stress as fluid is pushed away parallel to the wall. Right after impact ($20.07 \leq t \leq 20.25$) a thin layer of vorticity of opposite sign develops at the particle surface and at the wall, while vorticity in the wake of the particle decreases, though still present. At $t = 20.48$, the particle has reached its maximum height after the first bouncing and falls back again toward the wall. Afterwards ($t \geq 21.06$), the vorticity around the particle quickly disappears because of significant viscous dissipation.

The corresponding time evolution of the particle velocity is displayed in figure 5. Clearly, the particle reaches a steady-state velocity, denoted V_T , before bouncing on the wall. It can be noticed that before the collision effectively occurs the particle velocity decreases from V_T to an impact velocity, denoted V_C , which is about 12% less than V_T in the present case. During the bouncing, the particle velocity changes sign but does not recover its initial velocity. This rebound velocity is denoted V_R . Right after the impact, there is a strong decrease of the particle velocity followed by a milder trend. Finally, one can see on figure 5 a second rebound ($t \approx 21$) which is hardly detectable from the flow visualization.

The simulation presented in figures 4 and 5 were first repeated for two specific density ratios $\rho_p/\rho_f = 8$ and 16 (St and Re varying in the abovementioned range) and one specific Reynolds number $Re = 1$, without any lubrication model (18). We plot in figure 6 the restitution coefficient $\mathcal{E} \mathcal{E}_{max} = V_R/V_T$ (see figure 5 for definitions) as a function of Stokes number (22). For comparison, we included available experiment data of the rebound of a spherical inclusion with a wall or another particle. While the numerical results are in good agreement with experimental data for $St \geq 200$, the restitution coefficient is clearly overestimated at lower St . This can be attributed to the low resolution of the flow field when the gap between the particle and the wall is of the order of the grid size. As a consequence, the film pressure

stemming from the drainage of the liquid in the gap is underestimated so the particle rebound is artificially enhanced. This issue is overcome when one adds a lubrication force (18) in (3). Figure 7 shows the results obtained with the coupled IBM-DEM method with the lubrication model (18) for the case $\rho_p/\rho_f=8$. The numerical results fall in the range of the experimental data.

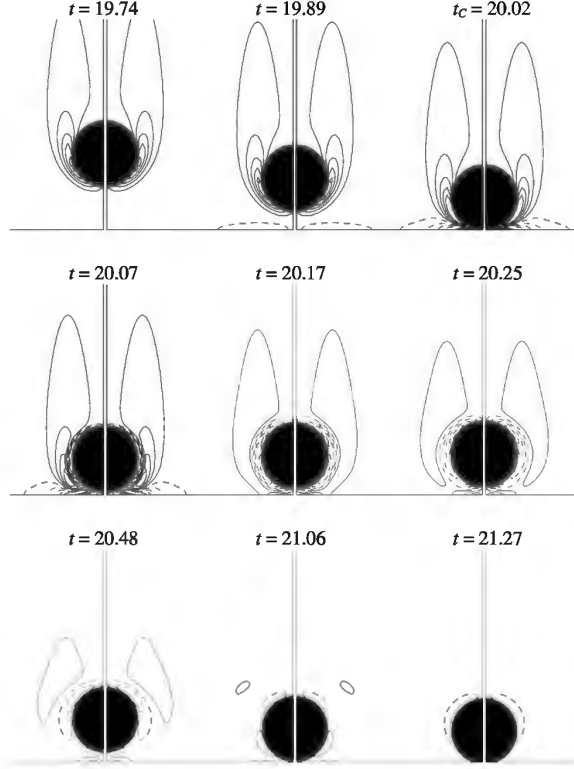


Figure 4: Vorticity field around a sphere impacting a wall ($\rho_p/\rho_f=8$, $St=53$, $Re\approx 60$, $D/\Delta z=20$). Contours levels are set from -17.8 to 17.8 in increments of 3.9. Here, time and vorticity are scaled by $(D/g)^{1/2}$ and $(g/D)^{1/2}$, respectively.

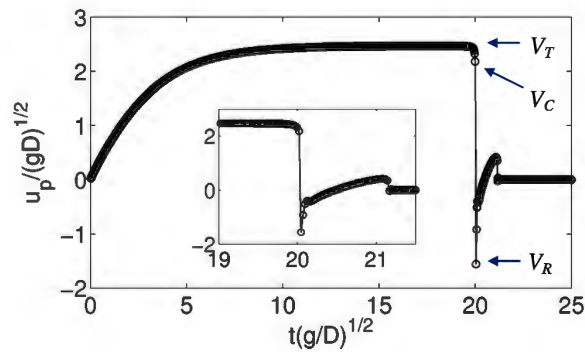


Figure 5: Temporal evolution of the particle vertical velocity (same case as figure 3). Inset: close-up view of the velocity during bouncing. Also defined are the particle terminal velocity V_T , the velocity at contact V_C and the rebound velocity V_R .

Overall, one may conclude from figure 7 that the present IBM-DEM method is able to reproduce the rebound of a particle in a viscous fluid provided a suitable lubrication model is added to compensate the inability of the flow solver to capture the small scale flow field in the gap during the film drainage.

A new model for the prediction of the effective coefficient of restitution

In this section, we propose a new model predicting the restitution coefficient $\varepsilon = -V_R/V_T$ observed in experiments without any adjustable constants. As shown later, this model only depends on two parameters, namely the Stokes number (22) and the relative surface roughness η/R . Some recent effort were done in attempting to predict the restitution coefficient thanks to models either based on lubrication theory (elasto-hydrodynamic model, Davis et al. 1986, Barnocky & Davis 1988; mixed contact model, Yang & Hunt 2008), or on a mass-spring analogy (Legendre et al. 2005, 2006). However, the first class of model fails to predict the restitution coefficient for the whole range of Stokes number, while the second class of model makes use of an adjusted constant.

Here we revisit both types of theory to derive a simple model which is able to capture reasonably well the observed restitution coefficients for the whole range of Stokes number (figure 7). The key idea is to decompose the sphere dynamics before and during impact into two stages. The first stage starts from a characteristic time at which the particle velocity begins to be influenced by the wall (i.e. for $\delta_n \approx R$, approximately, see figures 4-5 and corresponding discussions) up to the time at which collision occurs ($\delta_n=0$). During this stage, the particle is assumed (i) not to be deformed and (ii) to be slowed down by viscous forces generated by the displacement of fluid due to the presence of the wall. During the first stage, the particle velocity decreases from V_T to V_C , (see figure 5 for definition). In the second stage, the particle get deformed and bounces. During this stage, we assume that the particle kinetic energy is converted into energy of deformation and is only partially restored into kinetic energy because some of the energy has been dissipated by both inelastic deformation and viscous dissipation. During the second stage, the particle velocity goes from V_C to V_R .

In order to estimate the ratio V_C/V_T , we consider that the particle, at location x_p and of velocity u_p , is moving toward a flat wall in a fluid at rest and we assume that the particle is subject to the steady drag force which is balanced by the buoyancy force, the added-mass force and the lubrication force F_{lub} defined in (18) which, in the present case, becomes $F_{lub} = -6\pi\mu u_p R^2 / (\delta_n + \eta)$. The kinematic equations then become,

$$\frac{dx_p}{dt} = -u_p ; \quad (m_p + C_M m) \frac{du_p}{dt} = F_{lub} \quad (23a,b)$$

where m is the mass of the fluid contained in a sphere of radius R . Using the relation $x_p = R + \delta_n$, then dividing (23b) by (23a) in order to eliminate time, and integrating between $\delta_n=0$ ($u_p=V_C$) and $\delta_n=R$ ($u_p=V_T$), we find that

$$\frac{V_C}{V_T} = 1 + \frac{1}{St} \ln\left(\frac{\eta}{R}\right) \quad (24)$$

where we assumed that $R \gg \eta$. Regarding the second stage, we follow Legendre et al. (2005)'s analysis and use a mass-spring model to describe the deformation ξ of the particle where we take into account energy loss due inelastic deformation and viscous dissipation. The deformation of the particle is then governed by,

$$(m_p + C_M m) \frac{d^2 \xi}{dt^2} + (6\pi\mu RC + \gamma_n) \frac{d\xi}{dt} + k_n \xi = 0 \quad (25)$$

with initial conditions $\xi=0$ and $d\xi/dt=V_C$ when the particle impacts the wall. Recall that γ_n and k_n are the damping and stiffness coefficient of the soft-sphere mass-spring model, respectively. C is a coefficient which we estimate to be inversely proportional to the relative surface roughness of the particle, i.e. $C=R/\eta$. Integrating (25) with the corresponding initial conditions gives the classical solution $\xi(t)$ of a damped harmonic oscillator (not shown), with a half-period of oscillation

$$\tau = \pi \sqrt{\frac{m_p + C_M m}{k_n}} \frac{1}{\sqrt{1 - \frac{(3\pi\mu RC + \gamma_n/2)^2}{k_n(m_p + C_M m)}}} \quad (26)$$

(26) indicates that the larger the viscosity and/or γ_n , the larger τ , so that the contact time is larger accordingly, as expected. However, recent experiments of the impact of a solid sphere on a wall showed that the effective contact time remains finite and of the order of the contact time predicted by Hertz theory (considering no interaction with the surrounding fluid), in a large range of Stokes number $20 \leq St \leq 10^3$ (Legendre et al. 2006). Therefore, one can approximate (26) by $\tau \approx (m_p + C_M m)/k_n^{1/2}$.

Further assuming that the contribution of the lubrication force at impact $6\pi\mu R^2 V_C/\eta$ is of the same order as that of the elastic force $k_n \eta$ in the dissipation of energy, one can estimate R/η as a function of the fluid and particle properties as $R/\eta = (k_n/6\pi\mu V_C)^{1/2}$. Using this together with (26), the solution of (25) and the approximation $\tau \approx (m_p + C_M m)/k_n^{1/2}$, we can get an expression of the rebound velocity $V_R = d\xi(\tau)/dt$, as a function of the contact velocity V_C ,

$$\frac{V_R}{V_C} = -e_n \exp\left(-\frac{\pi/2}{\sqrt{St \times \beta(St, \eta/R)}}\right) \quad (27)$$

$$\beta(St, \eta/R) = 1 + \frac{1}{St} \ln\left(\frac{\eta}{R}\right) \quad (28)$$

Combining (24), (27) and (28), we find a new model for the prediction of the coefficient of restitution e'/e_{max} of a particle rebound in a fluid,

$$\frac{e'}{e_{max}} = \frac{-V_R/V_T}{e_n} = \beta(St, \eta/R) \exp\left(-\frac{\pi/2}{\sqrt{St \times \beta(St, \eta/R)}}\right) \quad (29)$$

As mentioned above, this new model only depends on two parameters, namely St and η/R . Note that here no adjustable

constant were needed. The model (29) is plotted in figure 7 for a wide range of relative surface roughness $10^{-6} \leq \eta/R \leq 10^{-3}$. Good agreement is observed for both small and large values of the Stokes number. Note that the sensitivity of (29) with respect to η/R is larger at moderate-to-small Stokes numbers. This is line with the dispersion of experimental results which is observed to be larger at low St .

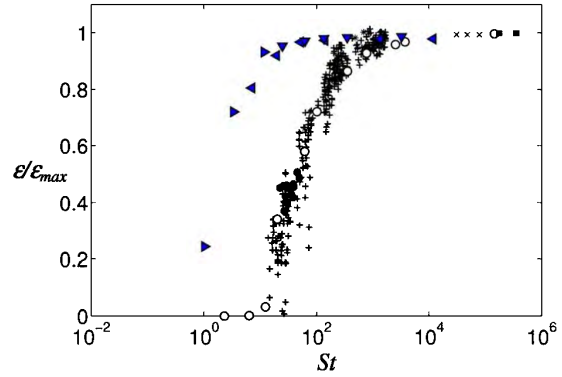


Figure 6: Restitution coefficient e'/e_{max} for spherical inclusions versus the Stokes number St . Present IBM-DEM simulations without lubrication force: ∇ , $\rho_f/\rho=16$; \blacktriangleleft , $\rho_f/\rho=8$; \blacktriangleright , $Re_p \approx 1$. Experiments with solid spheres: $+$, Joseph et al. 2001; \circ , Gondret et al. 2002; \times , Foerster et al. 1994. Experiments with drops: \bullet , toluene drops in water (Legendre et al. 2005); \blacklozenge , liquid drop in air (Richard & Quéré 2000). Other experiments: \blacksquare , spherical balloon filled with a mixture of water and glycerol (Richard & Quéré 2000).

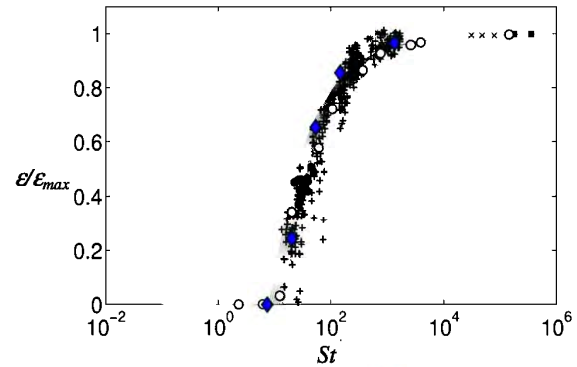


Figure 7: Same as figure 6: \blacklozenge , present IBM-DEM simulations with lubrication force (18) for $\rho_f/\rho=8$. —, present model (29) with various relative surface roughness $10^{-3} \leq \eta/R \leq 10^{-6}$.

Immersed granular flow on an inclined plane

The last case corresponds to the simulation of an immersed granular flow on an inclined plane, as those encountered in submarine avalanches. The simulation is performed in a three-dimensional (x,y,z) -computational domain of size $3D \times 3D \times 10D$ in the streamwise, spanwise and vertical directions, respectively, discretized with $30 \times 30 \times 100$ grid

points. We set the physical properties of the particle and the fluid so the density ratio is $\rho_p/\rho = 85$ and the Archimedes number $Ar = \rho(\rho_p - \rho)gD^3/\mu^2 = 1200$ ($Re = \rho u_p D/\mu \approx 10-100$). The collision parameters are the same as those used in figure 4. Periodic boundary conditions are imposed in the streamwise x -direction and no-slip boundary conditions are imposed elsewhere. The gravity vector makes an angle of 45° with the z -direction in the (x,z) -plane. Twenty quasi-monodispersed particles are initially randomly placed in the computational domain within a fluid at rest.

Figure 8 shows the temporal evolution of the granular flow. The particles first collapse thanks to gravity ($0 \leq t \leq 5$) to form a dense layer of particles which move as a sheet flow. The motion is sustained by the gravity since the angle of the inclined wall is well above the angle of avalanche ($\approx 30^\circ$ for spherical particles). In that case, the fluid is put in motion by the displacement of the particle as observed in avalanches. The present results with a somewhat modest spatial resolution open the way for a parametric study in the parameter space initial aspect ratio - initial packing with a larger number of better-resolved particles.

Conclusions

We presented a simple soft-sphere immersed-boundary method capable of describing the flow of a dense granular media evolving in a viscous fluid. Simulations of wall-particle collisions in a fluid are shown to be in good agreement with available experimental results for the whole range of investigated parameters, provided that a local lubrication model is used. A new model predicting the coefficient of restitution as a function of the Stokes number and the relative surface roughness of the particles has been proposed and was shown to reproduce reasonably well experimental data. Finally, simulations of dense granular flows in a viscous fluid are presented. Current effort is made to perform a parametric study in the parameter space initial aspect ratio - initial packing, in order to investigate immersed granular avalanches encountered in real situations.

Acknowledgements

The authors thank Annaig Pedrono for her support in the development of the immersed-boundary version of the Navier-Stokes solver used in this research. Some of the computational time was provided by the Scientific Groupment CALMIP (project P1027), the contributions of which is greatly appreciated.

References

- Barnocky, G. & Davis, R. H. 1988 Elastohydrodynamic collision and rebound of spheres: experimental verification. *Phys. Fluids* **31**, 1324-1329.
- Brenner, H. 1961 The slow motion of a sphere through a viscous fluid towards a plane surface. *Chem. Eng. Sci.* **16**, 242-251.
- Clift, R., Grace J. R. & Weber, M. E. 1978. In *Bubbles Drops and Particles*. Academic Press.

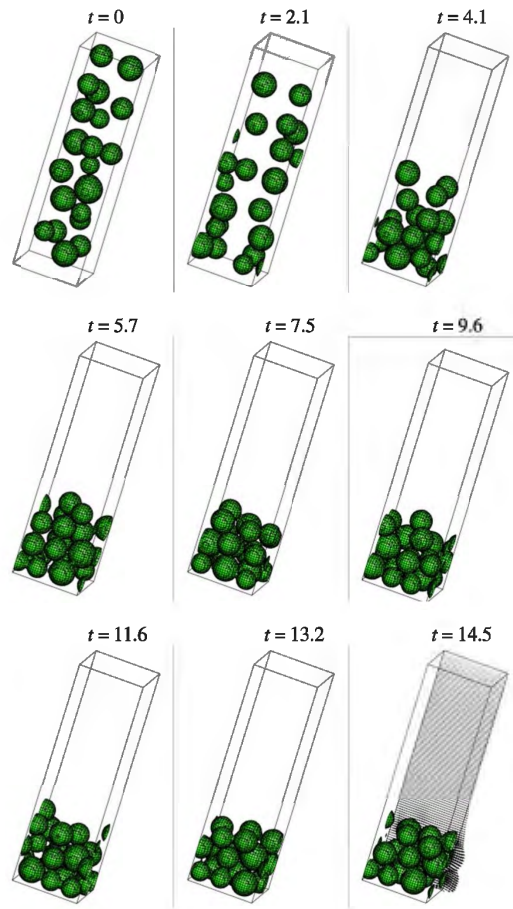


Figure 8: Simulation of an immersed granular flow on a inclined plane in a viscous liquid. Time is scaled by $(D/g)^{1/2}$. The grid resolution is made visible by lines plotted on the particles and the velocity field on a vertical plane at $t=14.5$.

- Davis, R. H., Serayssol, J. M. & Hinch, E. J. 1986 The elastohydrodynamic collision of 2 spheres. *J. Fluid Mech.* **163**, 479-497.
- Fadlun, E. A., Verzicco R. Orlandi P. & Mohd-Yusof, J. 2000 Combined immersed boundary finite-difference methods for three-dimensional complex flow simulations. *J. Comput. Phys.* **161**, 35-60.
- Foerster, S. F., Louge, M. Y., Chang, A. H. & Allia, K. 1994 Measurements of the collision properties of small spheres. *Phys. Fluids* **6**, 1108-1115.
- Goldhirsch, I. & C. Goldenberg, 2002 On the microscopic foundations of elasticity, *Eur. Phys. J. E.* **9**, 245-251.
- Gondret, P., M. Lance and L. Petit 2002 Bouncing motion of spherical particles in fluid, *Phys. Fluids* **14**, 643-652.
- Hu, H., Patankar N. & Zhu, N. 2001 Direct numerical simulation of fluid-solid systems using the arbitrary lagrangian eulerian technique. *J. Comput. Phys.* **169**, 427-462.

Joseph, G. , R. Zenit, L. Hunt and M. Rosenwinkel 2001 Particule-wall collisions in a viscous fluid, *J. Fluid Mech.* **433**, 329-346.

Kempe, T. & J. Fohlich, 2012 Collision modelling for the interface-resolved simulation of spherical particules in viscous fluids, *J. Fluid Mech.*, **709**, 445 – 489.

Kim, J., Kim D. & Choi, H. 2001 An immersed-boundary finite-volume method for simulations of flow in complex geometries. *J. Comput. Phys.* **171**, 132–150.

Legendre, D. C. Daniel and P. Guiraud 2005 Drop-wall bouncing in a liquid, *Phys. of Fluids*, **17**, 97-105.

Legendre, D., Zenit, R., C. Daniel and P. Guiraud 2006 A note on the modeling of the bouncing of spherical drops or solid spheres on a wall in viscous fluid, *Chem. Eng. Sc.* **61**, 3543-3549.

Moin, P. & Mahesh, K. 1998 Direct numerical simulation: a tool in turbulence research. *Ann. Rev. Fluid Mech.* **30**, 539–578.

Mougin, G. & Magnaudet, J. 2001 Path instability of a rising bubble. *Phys. Rev. Lett.* **88**, 014502.

Peskin, C. 2000 The immersed boundary method. *Acta Numerica* **11**, 479–517.

Richard, D. & Quéré D. 2000 Bouncing water drops. *Eurphysics Letters* **50**, 769-775.

Uhlmann, M. 2005 An immersed boundary method with direct forcing for the simulation of particulate flows. *J. Comput. Phys.* **209**, 448–476.

Yang, F.L. & M. L. Hunt, 2006 Dynamics of a particule-particule collisions in a viscous liquid, *Phys. Fluids* **18**, 121506.

Yuki, Y., Takeuchi S. & Kajishima, T. 2007 Efficient immersed boundary method for strong interaction problem of arbitrary shape object with self-induced flow. *J. Fluid Sci. Tech.* **2**, 1–11.